JCI insight

Antiretroviral treatment does not prevent extrapulmonary tuberculosis during SIV/Mtb coinfection in macaques

Collin R. Diedrich, Tara Rutledge, Janelle L. Gleim, Christopher Kline, Pauline Maiello, Jessica M. Medrano, H. Jacob Borish, Harris B. Chishti, Justin L. Gaines, Edwin Klein, Forrest Hopkins, Jacob E. Klein, Daniel Fillmore, Kara Kracinovsky, Jaime Tomko, Jennifer Schober, Sarah M. Fortune, Michael C. Chao, JoAnne L. Flynn, Zandrea Ambrose, Philana Ling Lin

JCI Insight. 2026;11(4):e199314. https://doi.org/10.1172/jci.insight.199314.

Research Article AIDS/HIV Immunology Infectious disease

Coinfection with both HIV and *M. tuberculosis* (Mtb) results in disseminated tuberculosis (TB) and accelerated HIV progression. Despite greater access to antiretroviral treatment (ART), it remains unclear whether suppression of HIV replication protects against severe Mtb infection. Here, using a macaque model of SIV/Mtb coinfection, we investigated whether treatment of SIV infection with ART influenced control of a subsequent Mtb challenge compared with SIV-infected macaques that were not treated with ART. Macaques were first infected with SIVB670, SIVB670 with ART, or saline followed by a low-dose Mtb inoculation with serial clinical and PET-CT imaging assessments. At necropsy, gross pathology, viremia, bacterial burden, and immunologic parameters were compared. SIV-TB animals had greater gross pathology and total bacterial burden than TB-only and SIV/ART/TB groups. However, despite normal blood CD4 counts and undetectable SIV RNA, SIV/ART/TB macaques showed similar clinical parameters and extrapulmonary involvement as SIV/TB animals. Analysis of barcoded-Mtb suggests that ART control of SIV replication did not prevent Mtb extrapulmonary dissemination. These data indicate that people living with HIV on ART remain at high risk of bacterial dissemination and extrapulmonary TB disease. Understanding the mechanisms of extrapulmonary spread and disease severity during HIV/TB coinfection remains an important issue.

Find the latest version:

https://jci.me/199314/pdf

JCI insight

RESEARCH ARTICLE

Antiretroviral treatment does not prevent extrapulmonary tuberculosis during SIV/Mtb coinfection in macaques

Collin R. Diedrich,[1,2] Tara Rutledge,[1,2] Janelle L. Gleim,[2,3] Christopher Kline,[2,3] Pauline Maiello,[2,3] Jessica M. Medrano,[1,2] H. Jacob Borish,[2,3] Harris B. Chishti,[2,3] Justin L. Gaines,[1] Edwin Klein,[4] Forrest Hopkins,[5] Jacob E. Klein,[2,3] Daniel Fillmore,[2,3] Kara Kracinovsky,[2,3] Jaime Tomko,[2,3] Jennifer Schober,[2,3] Sarah M. Fortune,[5] Michael C. Chao,[5] JoAnne L. Flynn,[2,3] Zandrea Ambrose,[2,3] and Philana Ling Lin[1,2]

[1]Department of Pediatrics, Children's Hospital of Pittsburgh of the University of Pittsburgh Medical Center, Pittsburgh, Pennsylvania, USA. [2]Center for Vaccine Research, [3]Department of Microbiology and Molecular Genetics, and [4]Division of Laboratory Animal Research, University of Pittsburgh School of Medicine, Pittsburgh, Pennsylvania, USA. [5]Department of Immunology and Infectious Diseases, Harvard T. H. Chan School of Public Health, Boston, Massachusetts, USA.

Coinfection with both HIV and *M. tuberculosis* (Mtb) results in disseminated tuberculosis (TB) and accelerated HIV progression. Despite greater access to antiretroviral treatment (ART), it remains unclear whether suppression of HIV replication protects against severe Mtb infection. Here, using a macaque model of SIV/Mtb coinfection, we investigated whether treatment of SIV infection with ART influenced control of a subsequent Mtb challenge compared with SIV-infected macaques that were not treated with ART. Macaques were first infected with SIVB670, SIVB670 with ART, or saline followed by a low-dose Mtb inoculation with serial clinical and PET-CT imaging assessments. At necropsy, gross pathology, viremia, bacterial burden, and immunologic parameters were compared. SIV-TB animals had greater gross pathology and total bacterial burden than TB-only and SIV/ART/TB groups. However, despite normal blood CD4 counts and undetectable SIV RNA, SIV/ART/TB macaques showed similar clinical parameters and extrapulmonary involvement as SIV/TB animals. Analysis of barcoded-Mtb suggests that ART control of SIV replication did not prevent Mtb extrapulmonary dissemination. These data indicate that people living with HIV on ART remain at high risk of bacterial dissemination and extrapulmonary TB disease. Understanding the mechanisms of extrapulmonary spread and disease severity during HIV/TB coinfection remains an important issue.

Introduction

Tuberculosis (TB), the disease caused by *Mycobacterium tuberculosis* (Mtb), is currently the most common infectious cause of death, leading to 1.23 million deaths in 2024 with 10.7 million new active TB cases (1). HIV is the greatest risk factor for TB, even when CD4 T cell counts are in the normal range, and HIV/Mtb coinfection accelerates progression of both TB and AIDS (2). Clinical manifestations of TB among people living with HIV (PLWHIV) often vary by degree of immune suppression. While pulmonary disease remains the most common clinical manifestation of TB, atypical presentations can occur and are often associated with low CD4 counts. Symptoms are often more subtle, chest radiographs can have atypical findings with negative sputum smears, and the rates of extrapulmonary disease (defined as TB pathology at anatomical sites outside of the thoracic cavity) are higher than HIV-naive individuals (3–5). The presence of extrapulmonary TB is more likely to be diagnosed in HIV/Mtb coinfected people and is associated with increased mortality (6).

Antiretroviral treatment (ART) to control HIV replication has dramatically improved HIV and HIV/Mtb coinfection care, especially as it is now available in up to 77% of PLWHIV (1). Delays in ART and low CD4 T cell counts correlate with increased TB incidence over time (1, 7, 8), and ART has been shown to reduce mortality from TB and the overall incidence of TB (9–11). Among HIV/Mtb coinfected individuals, ART can prevent or remedy the loss of CD4 T cells (7, 12, 13), improve Mtb-specific CD4 and CD8 T cell responses (14), and reduce macrophage dysfunction (15). However, ART only partially ameliorates the HIV-induced increase in susceptibility to TB (16), as PLWHIV on ART are still more susceptible to TB than

Conflict of interest: SMF is a nonexecutive director of Oxford Nanopore Technologies.

Copyright: © 2026, Diedrich et al. This is an open access article published under the terms of the Creative Commons Attribution 4.0 International License.

Submitted: August 19, 2025
Accepted: December 23, 2025
Published: February 23, 2026

Reference information: *JCI Insight*. 2026;11(4):e199314. https://doi.org/10.1172/jci.insight.199314.

HIV-uninfected individuals (17–19). The mechanisms by which HIV increases susceptibility to TB and why ART only partially reduces that risk are not well understood. It was initially presumed that a low CD4 count was the primary cause of the increase in TB susceptibility in PLWHIV (12), yet we and others have shown that there are CD4-independent risks associated with SIV-induced TB pathogenesis (20–24). Human cohort studies are challenging, as the order in which the infections occur (i.e., primary versus secondary HIV infection) and the duration of each infection are often unknown. For example, acute Mtb infection after chronic HIV infection may lead to worse severity than longstanding asymptomatic Mtb infection (latent) and subsequent acute HIV infection. To dissect these factors, highly controlled animal models to interrogate the phenomena and mechanisms of pathogenesis are beneficial.

Nonhuman primate (NHP) models of TB recapitulate many key features of human Mtb infection (25, 26), and we and others have shown that they can be productively infected with SIV to better understand HIV-Mtb coinfection (20–23, 27, 28). While many studies in NHP have addressed the role of SIV infection induced reactivation of latent Mtb infection (22, 23, 28, 29), to the best of our knowledge, this is the first study to address the influence of SIV infection aggressively controlled with ART and subsequent Mtb infection. Here, cynomolgus macaques were infected with SIV with or without ART and subsequently infected with Mtb to determine the influence of SIV replication or ART suppression of SIV on susceptibility to acute Mtb infection, using a barcoded strain of virulent Mtb. Our data confirm that SIV increases TB pathology and influences immunological functions. Although ART reduced pulmonary TB pathology, it did not prevent extrapulmonary spread of TB.

Results

SIV/ART/TB animals developed similar signs of TB disease as SIV/TB with immune activation. To address the effect of ART controlled viral suppression on SIV/Mtb coinfection, NHP were randomized into 4 groups: TB-only, SIV/TB, SIV/ART/TB, and SIV-only. SIV infection occurred for 16 weeks prior to Mtb infection with a subset of animals initiated on ART at day 3 of SIV infection, based on prior studies in which viral replication was suppressed despite established viral tissue reservoirs (30) (Figure 1A). Subsequent Mtb infection was planned for 12 weeks in all relevant groups. Serial positron emission tomography using 18-flourodeoxyglucose (FDG) probe and computed tomography (PET-CT) imaging and clinical, immunologic, and bacterial outcomes were compared at necropsy. We focused our comparisons between SIV/TB and SIV/ART/TB groups with secondary analyses including TB- and SIV-only groups.

Animals randomized to SIV infection without ART showed substantial reductions of CD4 T cells in blood, airways, and tissues (Figure 1B and Supplemental Figure 1; supplemental material available online with this article; https://doi.org/10.1172/jci.insight.199314DS1). Plasma viremia peaked at 1 week after infection and reached a setpoint by approximately 4 weeks (Figure 1B). The level of plasma SIV RNA among SIV/TB NHP was similar to the SIV-only animals. Sustained suppression of SIV replication occurred by 3 weeks of ART in the SIV/ART/TB NHP. This effectively prevented the loss of CD4 T cells within multiple compartments, resulting in significantly higher CD4 T cells counts in the blood, airway, and peripheral lymph nodes compared with SIV/TB NHP across all time points before and after Mtb infection (Figure 1B and Supplemental Figure 1). SIV-only and SIV/TB NHP also maintained similar CD4 T cell frequencies across all time points both before and during Mtb infection in blood, airway, and peripheral lymph nodes. Reductions in CD4 T cells in the SIV only and SIV/TB NHPs were associated with higher CD8 T cell counts (Supplemental Figures 1 and 2).

After Mtb challenge, both SIV/TB and SIV/ART/TB macaques displayed more clinical and immunologic signs of early Mtb infection than animals with Mtb infection alone (Figure 1C). To quantify and compare clinical signs of disease, we modified our previously published clinical scoring system (31) to numerically quantify signs of TB disease (see methods) (Figure 1C and Supplemental Figure 3). Peaking at 4–6 weeks after Mtb infection, 40% of the TB-only NHPs developed at least 1 sign of TB similar to previously published studies (25). However, 60%–90% of animals in the SIV/ART/TB and SIV/TB groups had at least 1 sign of disease at 4–6 weeks that continued throughout infection, often with both microbiologic markers and clinical signs of disease (Figure 1C and Supplemental Figure 3). We measured markers of immune activation, soluble CD14 (sCD14) (macrophage activation marker) and sCD163 (monocyte/macrophage scavenger receptor), often observed in humans with HIV/Mtb coinfection (32). Both the SIV/ART/TB and SIV/TB NHP had significant elevations in sCD14 after Mtb infection but only the SIV/TB group had increased levels of sCD163 (Figure 1, D and E). Erythrocyte sedimentation rate (ESR), a marker of systemic inflammation, can

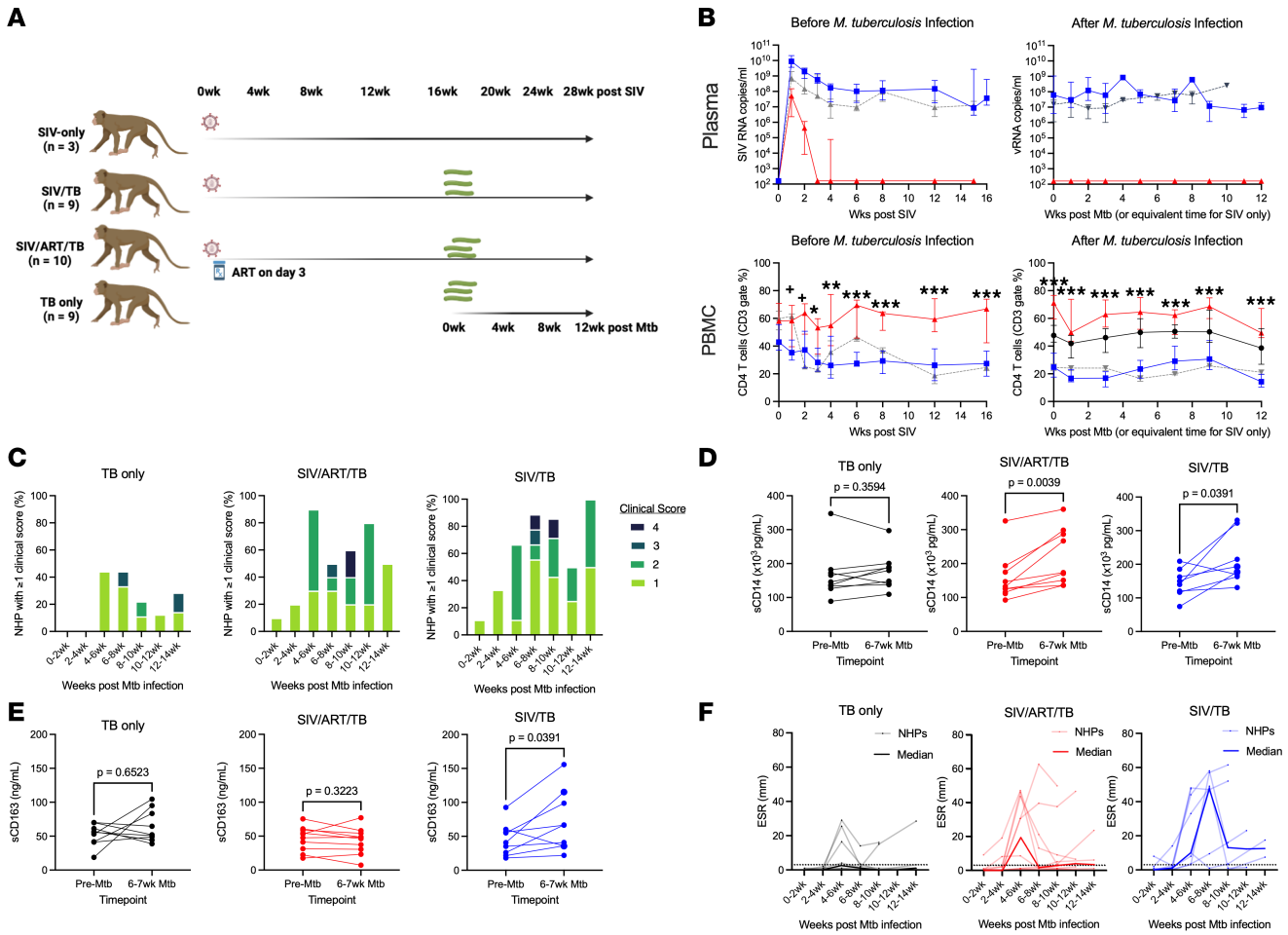

Figure 1. Study design and markers of disease. (**A**) Adult cynomolgus macaques were randomized to receive either SIV infection alone (n = 3), SIV infection for 16 weeks and then *M. tuberculosis* (Mtb) challenge (n = 9), SIV with antiretroviral treatment (ART) for 16 weeks and then Mtb challenge (n = 10), or Mtb infection alone (n = 9). ART was continued throughout the course of SIV and Mtb infection. Mtb infection (low dose Erdman) progressed for 12 weeks with serial blood, airway and lymph node sampling and PET-CT performed. (**B**) Serial SIV RNA plasma levels before and after Mtb infection and serial frequencies of CD4 T cells in the peripheral blood are shown. Median with IQR error bars shown. (**C**) Clinical scores within each treatment group are shown over the course of Mtb infection. (**D** and **E**) Interval change in immune activation markers, sCD14 and sCD163, are shown by group. Limit of detection for sCD14 is 125 pcg/mL and sCD163 is 0.469 ng/mL. (**F**) Erythrocyte sedimentation rates (ESR) during the course of infection by experimental group are shown. Each light-colored line represents a single animal over time; dark lines represent median at each time point. Normal range is 0–2 mm. (**B**) Statistical analysis was restricted to compare only SIV/ART/TB and SIV/TB groups. Mann-Whitney U test run at each time point and adjusted for multiple comparisons by Holm-Šídák method ($0.05 < {}^{+}P < 0.10$, $0.01 < {}^{*}P < 0.05$, $0.001 < {}^{**}P < 0.01$, ${}^{***}P < 0.001$). Black, TB-only; Blue, SIV/TB; Red, SIV/ART/TB; Gray, SIV-only. (**D** and **E**) Wilcoxon matched-pairs signed rank test used for analysis in **B** and **C**. TB-only (n = 9), SIV/ART/TB (n = 10), SIV/TB (n = 8–9).

be increased transiently during acute Mtb or SIV infection and remain elevated with worsening TB disease (25). In the TB-only group, the median ESRs were normal throughout Mtb infection, although there were increases in some animals (26). Conversely, SIV/TB NHP maintained high ESRs starting at 4–6 weeks after Mtb infection (median = 10 mm IQR$^{25–75}$, 3.25–45.75, n = 9), peaking at 6–8 weeks (47.5 mm, 3.125–55, n = 8) and many NHPs had elevated ESR thereafter (Figure 1F). SIV/ART/TB animals experienced high ESRs at 4–6 weeks after Mtb infection (19.5 mm, 0.875–44.13, n = 10) and remained slightly above normal levels thereafter. Interestingly, SIV/TB animals had higher plasma levels of Th1 cytokines (e.g., IL-12, IL-2) and IP-10 (CXCL10) before and during early Mtb infection compared with TB-only groups and/or SIV/ART/TB (Supplemental Figure 4). None of the TB-only and SIV/ART/TB animals reached humane endpoints prior to their predetermined time of necropsy after Mtb challenge (12 weeks). In contrast, the SIV/TB animals median time to necropsy was 8.9 weeks (Supplemental Figure 5).

ART did not prevent extrapulmonary dissemination of TB among SIV/ART/TB macaques. At necropsy, inflammation in the lungs and thoracic lymph nodes appeared greater in SIV/TB animals (Figure 2A). PET-CT–identified lung granulomas and other sites of disease progression were tracked during the

course of Mtb infection. Greater total lung inflammation (FDG activity) is noted in the SIV/TB groups at 8 and 12 weeks after Mtb infection (Figure 2B). At necropsy, SIV/TB NHP had greater overall TB pathology, especially in the lungs and extrapulmonary sites, compared with TB-only NHP (Figure 3A). However, SIV/ART/TB NHP had greater extrapulmonary involvement than the TB-only group (Figure 3B). A higher proportion of SIV/TB NHP developed TB pneumonia (indicating severe disease) compared with the TB-only and SIV/ART/TB NHP groups (78%, 20%, and 30%, respectively; $P = 0.03$) (Supplemental Figure 6A). Total bacterial burden (including lung and thoracic lymph node) among SIV/TB animals was higher than the TB-only and SIV/ART/TB groups (Figure 3C). Individual Mtb bacterial growth per lung granuloma varied across groups (Supplemental Figure 6, B and C). SIV/TB animals had higher CFU per lung granuloma (and total live and killed Mtb measured by chromosomal equivalents [CEQ]) indicating increased growth and/or reduced killing than the SIV/ART/TB and TB-only groups (Figure 4). Higher Mtb growth was also present in thoracic lymph nodes (with and without granulomas being present) in SIV/TB NHP compared with SIV/ART/TB and TB-only NHP (Figure 4). While it is not surprising that SIV infection increases overall pathology and Mtb growth within NHP, early control of SIV replication with ART appeared to prevent disease progression in the lungs and lymph node but did not ameliorate the dissemination of Mtb to extrapulmonary sites.

SIV-induced T cell changes are not completely ameliorated by ART. Given that peripheral blood responses do not accurately reflect those in the lung, we focused on the immunological responses in lung granulomas (33). Reduced frequency and total CD4 T cells were noted within lung granulomas of SIV/TB NHP but were preserved in SIV/ART/TB NHP (Figure 5, A and B). Similarly, the absolute number of HLA-DR expressing CD4 T cells was lower in the SIV/TB NHP compared with the other cohorts (Figure 5, C and D). Given the reduction in CD4 T cells in SIV/TB granulomas, it is not surprising that higher frequencies of CD8 T cells were observed in this group compared with others. The frequencies of CD8 T cells (though not total numbers) producing any Th1 cytokine (TNF, IFN-γ, or IL-2) were higher in the SIV/TB and SIV/ART/TB granulomas compared with TB-only NHP, possibly due to increased bacterial burden and stimulation by SIV or Mtb antigens (Figure 5, E and F) (though not among SIV/ART/TB groups). A higher percentage (but not total cells) of CD8 T cells producing IL-10 was also observed in SIV/ART/TB and SIV/TB NHP compared with TB-only NHP (Figure 5, G and H). Greater CD4 T cell expression of CD38 (activation marker and T cell regulator) and reduced IL-17 was observed among the SIV/TB NHP compared with TB-only controls (Supplemental Figure 7), which has been observed in blood of HIV/Mtb coinfected humans (34). We also utilized t-SNE to visualize more complex cell populations (Supplemental Figure 8) on a subset of samples that were available. Subtle shifts in phenotypic character among the CD4 and CD8 populations between the TB-only and the SIV (± ART) groups were noted, though they were not statistically significant, given the limited sample size.

Thoracic lymph nodes play an important role in T cell priming that is critical to the adaptive immune response and can harbor both Mtb and SIV (35, 36). While the frequency of CD4 T cell among SIV/TB lymph nodes was significantly lower than other groups (and the frequency of CD8 T cells consequently higher), the SIV/ART/TB animals had higher CD4 T cells than the other groups (Supplemental Figure 9). CD4 and CD8 T cells expressing CD38 in thoracic lymph nodes were significantly higher in SIV/TB NHP compared with TB-only and SIV/ART/TB NHP. Lastly, greater CD4 T cell expression of the degranulating protein CD107a was observed in the SIV/TB group compared the other groups. Based on t-SNE visualization of a subset of samples, subtle changes in surface marker and functional phenotypes were noted in both CD4 and CD8 populations in the lymph nodes (Supplemental Figure 10). Overall, thoracic lymph node T cell responses among SIV/ART/TB groups were more similar to the TB-only groups.

ART did not prevent Mtb-barcode dissemination to extrapulmonary sites. While it was clear that there was greater dissemination in the SIV/TB animals, we were surprised to see increased extrapulmonary dissemination in the SIV/ART/TB animals (Figure 6), prompting further analysis. We tracked the Mtb barcodes with PET-CT images across time points to compare bacterial establishment and dissemination within and across experimental groups (37). There was no difference in the number of unique barcodes established between each cohort (Figure 7A). There was no difference in the number of unique barcodes observed in early lung granulomas (granulomas established at 4 weeks after Mtb challenge by PET-CT) among the different cohorts (Figure 7B). Nor were there differences in unique barcode counts in thoracic lymph nodes across all groups (Figure 7C). However, both SIV/ART/TB and SIV/TB animals had

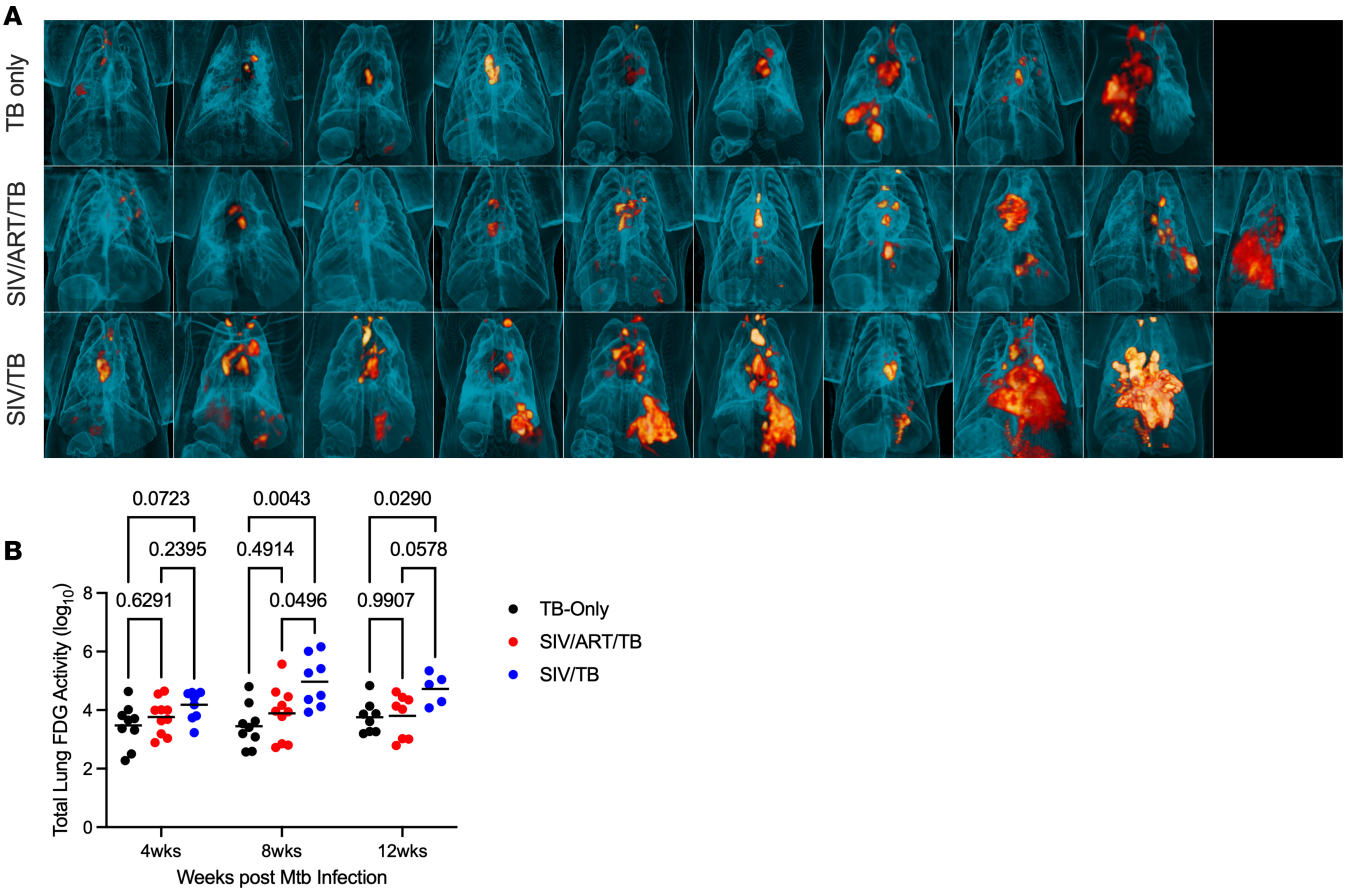

Figure 2. PET-CT images of tuberculosis-involved lung and thoracic LN at necropsy. (**A**) Top row, TB-only; middle row, SIV/ART/TB; bottom row, SIV/TB. Images are arranged in each group by total CFU (lowest CFU of the group on the left and highest on the right). (**B**) Total lung FDG activity is presented at 4, 8, and 12 weeks after Mtb infection for each cohort. Each dot represents an animal at each time point, and lines represent means. A mixed-effects analysis was utilized with Tukey's multiple-comparison test *P* values are shown.

greater numbers of barcodes shared between extrapulmonary and thoracic lymph node sites compared with the TB-only NHP (Figure 7D). Given that there are multiple thoracic lymph nodes (e.g., bilateral hilar and carinal lymph nodes) and extrapulmonary sites (e.g., liver, spleen, kidney), we examined the proportion of tissues in each compartment that shared barcodes. Again, both the SIV/ART/TB and SIV/TB NHPs had greater proportions of tissues sharing barcodes than the TB-only animals (Figure 7, E and F). No differences were observed in the overall diversity of barcodes within each animal based on treatment group (Supplemental Figure 11). In short, unexpectedly SIV did not influence the establishment of Mtb infection; we expected a greater number of unique barcodes in SIV/TB NHPs compared with other groups. Thus, while initial Mtb infection in the lungs and thoracic lymph nodes was unchanged, SIV infection was associated with greater dissemination to thoracic lymph nodes and extrapulmonary compartments, resulting in greater spread of Mtb independent of ART suppression.

Discussion

In low TB endemic countries like the United States, reactivation accounts for most TB cases (38). For this reason, many NHP studies have focused on SIV-induced reactivation of latent Mtb infection (22–24, 28, 29). However, the majority of TB cases (at least 70% in some reports) in high endemic areas are attributed to recent transmission (39–41). Since HIV is highly prevalent in TB endemic areas with 77% of PLWHIV having access to ART (1), we therefore focused on the clinical scenario in which PLWHIV would develop primary Mtb infection. Specifically, we aimed to elucidate the influence of aggressive ART treatment of SIV/Mtb coinfection on Mtb disease pathogenesis using the NHP model. ART displayed remarkable efficacy in controlling SIV replication and preventing severe pathology associated with SIV/Mtb coinfection (as others have observed without ART) (42–44). However, it remained ineffective in mitigating

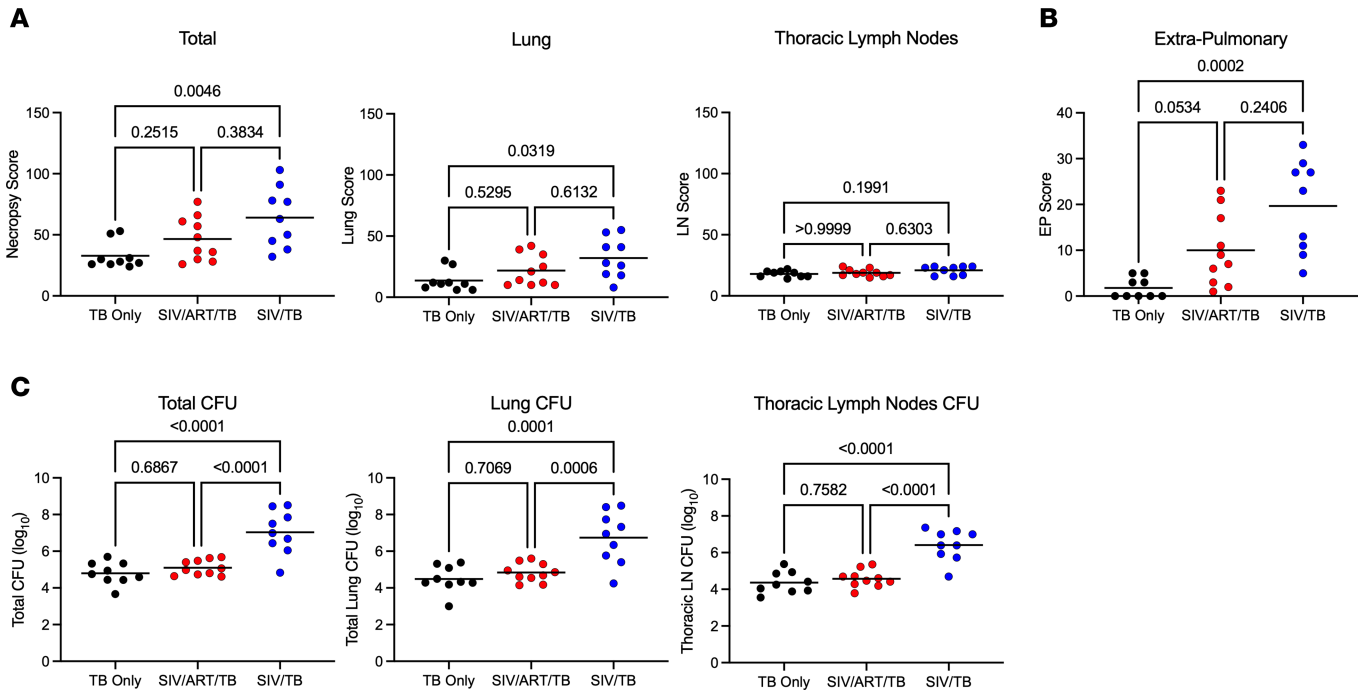

Figure 3. Gross pathology and Mtb burden at necropsy. (**A**) Tuberculosis-associated gross pathology is estimated using a quantitative score at necropsy (necropsy score) that includes disease specific to the lung, lymph node, and extrapulmonary sites. (**B**) Tuberculosis-associated extrapulmonary gross pathology and Mtb growth from these sites is used to estimate extrapulmonary score for each animal at necropsy. (**C**) Total bacterial burden, lung bacterial burden, and thoracic LN burden are shown across experimental groups. Lines represent means; each dot represents an animal. Kruskal-Wallis test with Dunn's multiple-comparison–adjusted *P* values reported in **A** and **B**. One-way ANOVA with Tukey's multiple-comparison adjusted *P* values reported in **C**. TB-only (n = 9), SIV/ART/TB (n = 10), SIV/TB (n = 9).

bacterial dissemination to extrapulmonary sites. There was a noticeable convergence in clinical signs of TB between SIV/TB and SIV/ART/TB groups that we speculate is due to the modified immunological response, including immune activation as seen by sCD14, in the ART group. Both SIV/TB and SIV/ART/TB NHP cohorts had elevated systemic inflammatory markers (ESR), early detection of Mtb growth from gastric aspirates (GA) or BAL, and other signs of systemic illness. These clinical manifestations of TB are correlated with increased TB pathology (22, 45, 46). Not surprisingly, CD4 T cells from SIV/TB NHPs were significantly lower in the blood, airways, and granulomas compared with other groups. The reduced number of HLA-DR$^+$ CD4 T cells observed within the SIV/TB NHP is consistent with the HIV literature in which HIV exhibits a preference for infecting HLA-DR$^+$ CD4 T cells (47). While early ART treatment prevented the loss of CD4 T cells, Th1 profiles and IL-10 expressing CD8 T cells from granulomas were more similar to SIV/TB animals compared with TB-only controls (Figure 5 and Supplemental Figure 7). We did not focus on the macrophage or neutrophil responses, but in a recent study of PLWHIV on sustained ART treatment, alveolar macrophages were found to have impaired TNF signaling and macrophage–T cell crosstalk (48). These data would suggest that ART does not ameliorate innate responses that are likely to be important in Mtb infection.

These studies provide insights into Mtb dissemination during SIV/Mtb coinfection with and without ART. Remarkably, primary SIV infection did not increase the establishment of Mtb infection, as the number of unique barcodes was similar across groups. Similar proportions of barcodes were found in the early granulomas and thoracic lymph nodes (the first sites of Mtb dissemination). However, SIV/TB and SIV/ART/TB NHPs had more unique barcodes shared between extrapulmonary and thoracic lymph node sites and greater proportions of tissues sharing these barcodes within the thoracic lymph nodes and extrapulmonary sites compared with TB-only (Figure 6); these findings support increased dissemination in SIV-infected macaques regardless of early and sustained ART. Notably, others have reported that the lymphatic system likely plays a pivotal role in Mtb dissemination (49) and that radiographic evidence of necrotic lymph nodes is associated with disruptions in lymph node pathology (50). This increased extrapulmonary dissemination without overt increased Mtb growth in thoracic lymph

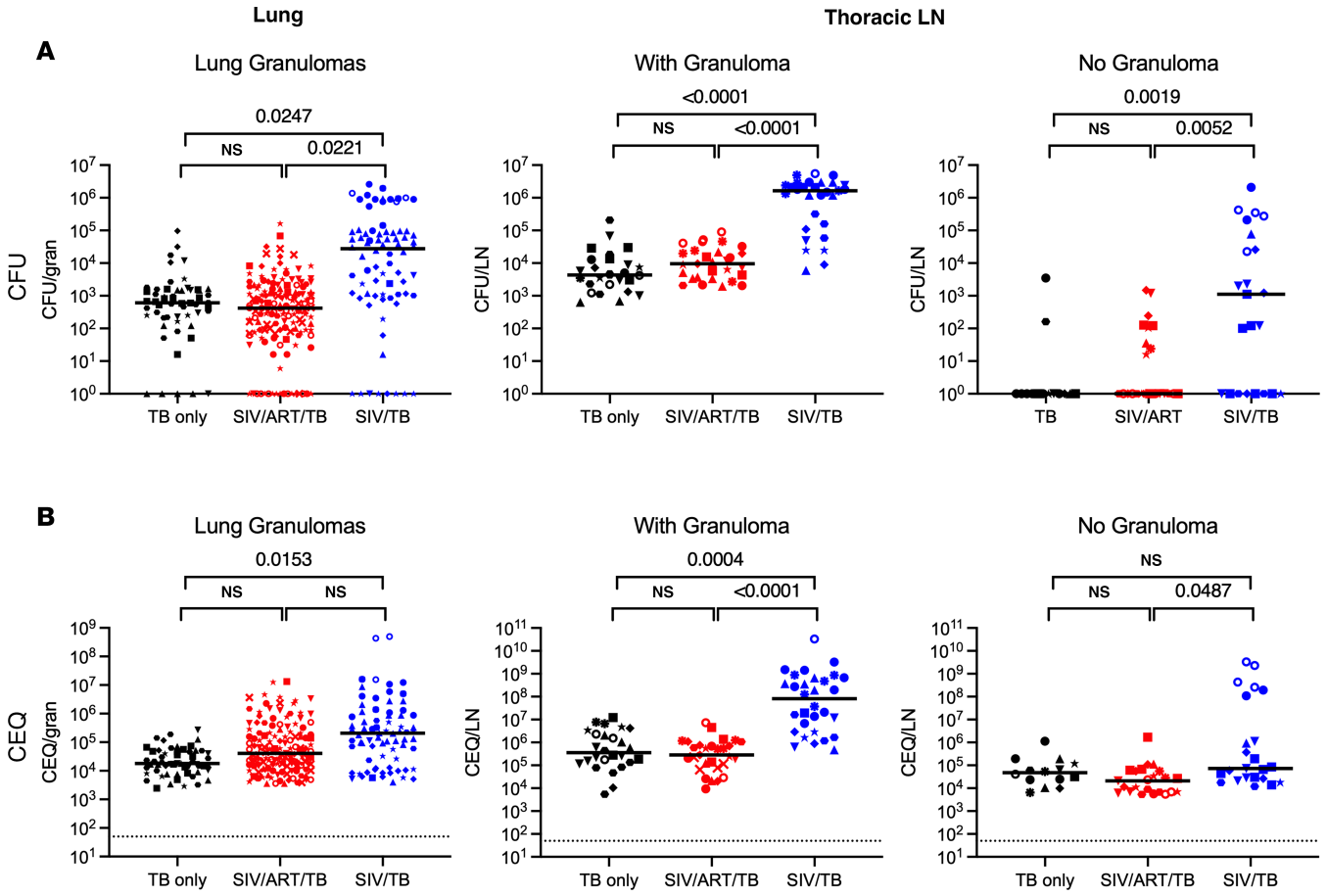

Figure 4. Comparison of viable and total (viable and killed) Mtb per granuloma by group. (**A**) Viable Mtb growth (CFU) by experimental group in lung granulomas and thoracic lymph nodes (with and without granuloma) are shown. (**B**) Total Mtb burden includes both viable and killed Mtb that is measured by chromosomal equivalents (CEQ) in lung granulomas and thoracic lymph nodes. Mixed effect model (animal as a random effect and treatment group as a fixed effect) was used; Tukey HSD adjusted *P* values (for $P < 0.10$) reported. Each dot represents an individual sample (granuloma or lymph node), and each symbol represents a different animal; lines represent medians.

nodes and lung suggests that Mtb dissemination may be driven by factors beyond bacterial load alone. Notably, the comparable Mtb growth in lung and thoracic lymph node compartments points to a previously unrecognized mechanism of SIV-mediated dissemination that persists despite ART intervention. We hypothesize that, once Mtb seeds the thoracic lymph node or extrapulmonary sites, SIV facilitates greater spread of Mtb within those specific anatomic compartments, which can result in increased bacterial burden. These findings raise important conceptual questions about the immune factors required to prevent dissemination from specific compartments (e.g., lung, lymph node), particularly as they relate to extrapulmonary spread of Mtb.

Little is known about the pathogenesis of extrapulmonary disease, though it is often correlated with an increase in mortality especially in coinfected individuals (51). PLWHIV are more likely to develop extrapulmonary TB than HIV uninfected individuals (4, 51, 52), especially those with low peripheral CD4 T cells (6, 53). The widespread adoption of ART has resulted in a reduction in miliary and disseminated TB (54), although other forms of extrapulmonary TB (e.g., lymphadenitis, meningitis) remain (55). In fact, PLWHIV treated with ART who subsequently develop TB appear to be at a heightened risk of extrapulmonary TB (56). In those individuals already on ART at the time of TB diagnosis, the median duration until the diagnosis was approximately 15 weeks (56), a timeframe mirroring the observations in our current study where all NHP were necropsied between weeks 8 and 13. We would hypothesize that the immune changes that occur with ART, like HIV-immune reconstitution inflammatory syndrome (18), may alter clinical signs and symptoms, prompting the evaluation of extrapulmonary TB similar to the "unmasking TB" scenario where a more robust immune response results in more clinical manifestations of existing disease that was previously asymptomatic.

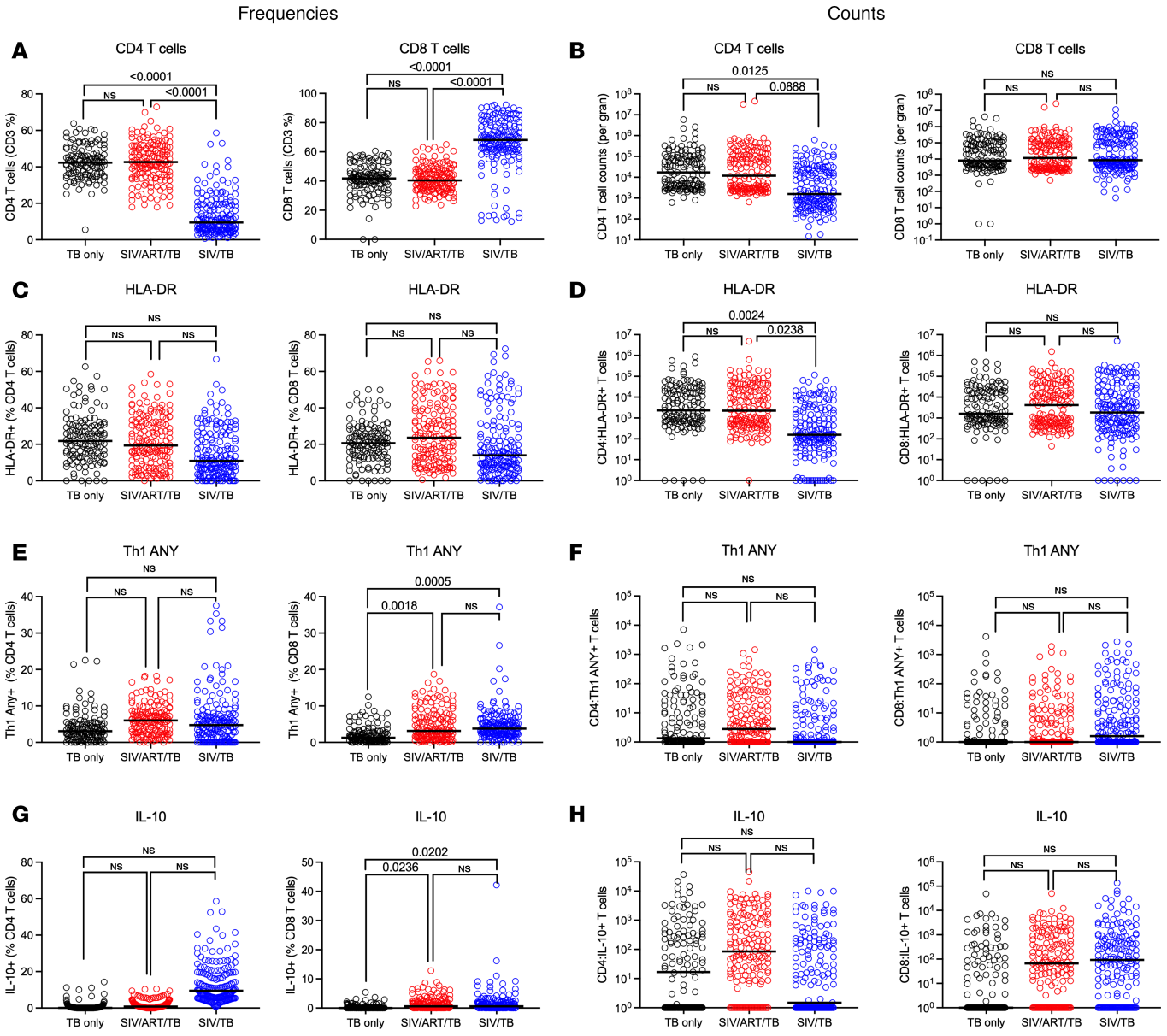

Figure 5. Immunophenotyping of granulomas by experimental group. (**A** and **B**) Frequency and absolute numbers of CD4 and CD8 T cells per granuloma are shown. (**C** and **D**) Frequency and absolute number of HLA-DR expressing CD4 and CD8 T cells within granulomas are shown. (**E** and **F**) Frequency and absolute numbers of the CD4 and CD8 T cells expressing any Th1 cytokine (at least one of the following: IFN-γ, TNF, or IL-2) within granulomas is shown. (**G** and **H**) Frequency and absolute numbers of IL-10 expressing CD4 and CD8 T cells is shown. Each circle represents a granuloma; lines are medians. Mixed effect model (animal as a random effect and treatment group as a fixed effect) was used; Tukey HSD adjusted *P* values (for $P < 0.10$) reported.

While these studies reveal important insights into the complexities of HIV/Mtb coinfection, there are limitations to our studies. We primarily focused on T cell responses, though it is very possible that other cell types (e.g., macrophages, neutrophils) and mechanisms are contributing to these changes and are worth examining in future studies. Given limited resources, the numbers of animals in each group were powered based on total bacterial burden, so our secondary analyses, which included more subtle signs to assess factors that might protect against extrapulmonary disease, were insufficiently powered. In our case, the duration of SIV infection was 4 months rather than the years that likely occur in humans. Furthermore, ART began at day 3 after SIV infection, which could be considered an unusual clinical scenario in humans, where HIV ART is often initiated months to years after HIV infection. In clinical practice, there are uncertainties in the precise timing of HIV and Mtb infections, the duration of these coinfections, and adherence to ART. Granulomas likely act as viral reservoirs, and there has been an increasing awareness that HIV proteins like gp120 and other proteins can be shed despite HIV suppression and lead to immune

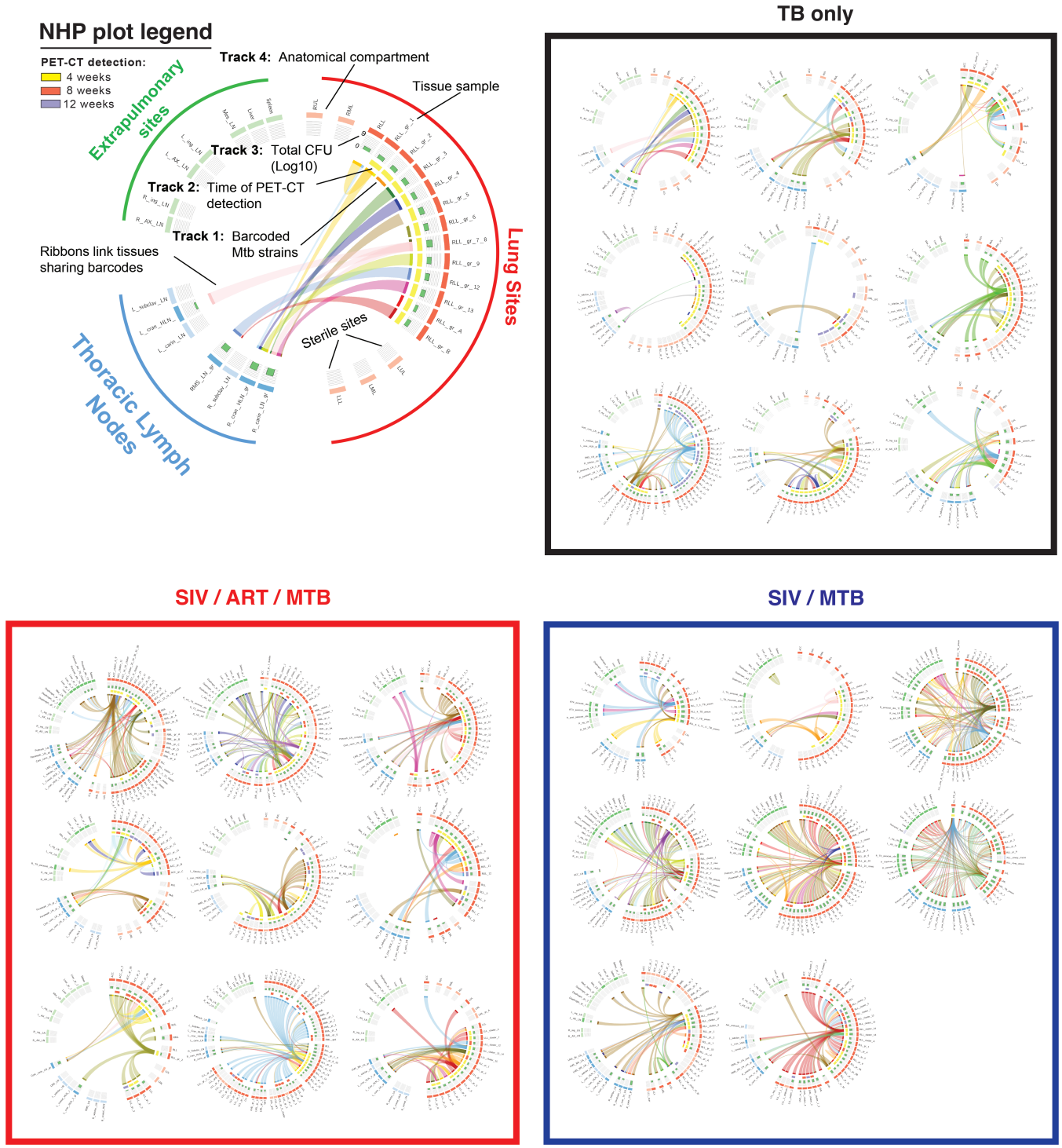

Figure 6. Dissemination and unique Mtb barcode tracking. Barcoded Mtb infection of and dissemination across tissues. Circos plots were generated to visualize the barcoded Mtb strains identified in each animal and separated by treatment groups. As described in a key (top left), each color represents a different barcode sequence identified and barcodes shared across tissues are linked by a ribbon (Track 1). Lung granulomas that were detected by PET-CT at 4 (yellow), 8 (red), or 12 weeks (purple) after infection are indicated in Track 2; and the total bacterial burden per tissue sample at necropsy is provided as histograms in Track 3. Sampled tissues are organized by anatomical compartment, including those from lungs (red), thoracic lymph nodes (blue), and extrapulmonary sites (green). Lung sites are also grouped by lung lobe: RUL, right upper lobe; RML, right middle lobe; RLL, right lower lobe; LUL, left upper lobe; LML, left middle lobe; LLL, left lower lobe; Acc, accessory lobe. Sites in lighter shading represent sampled tissues that were found to be sterile.

dysfunction, potentially influencing innate response to Mtb infection (57); future studies could identify whether the presence of provirus in granulomas or lymph nodes alters the immune state. Importantly, it is possible that the immune influence that increases the risk of Mtb dissemination could be attributed to the

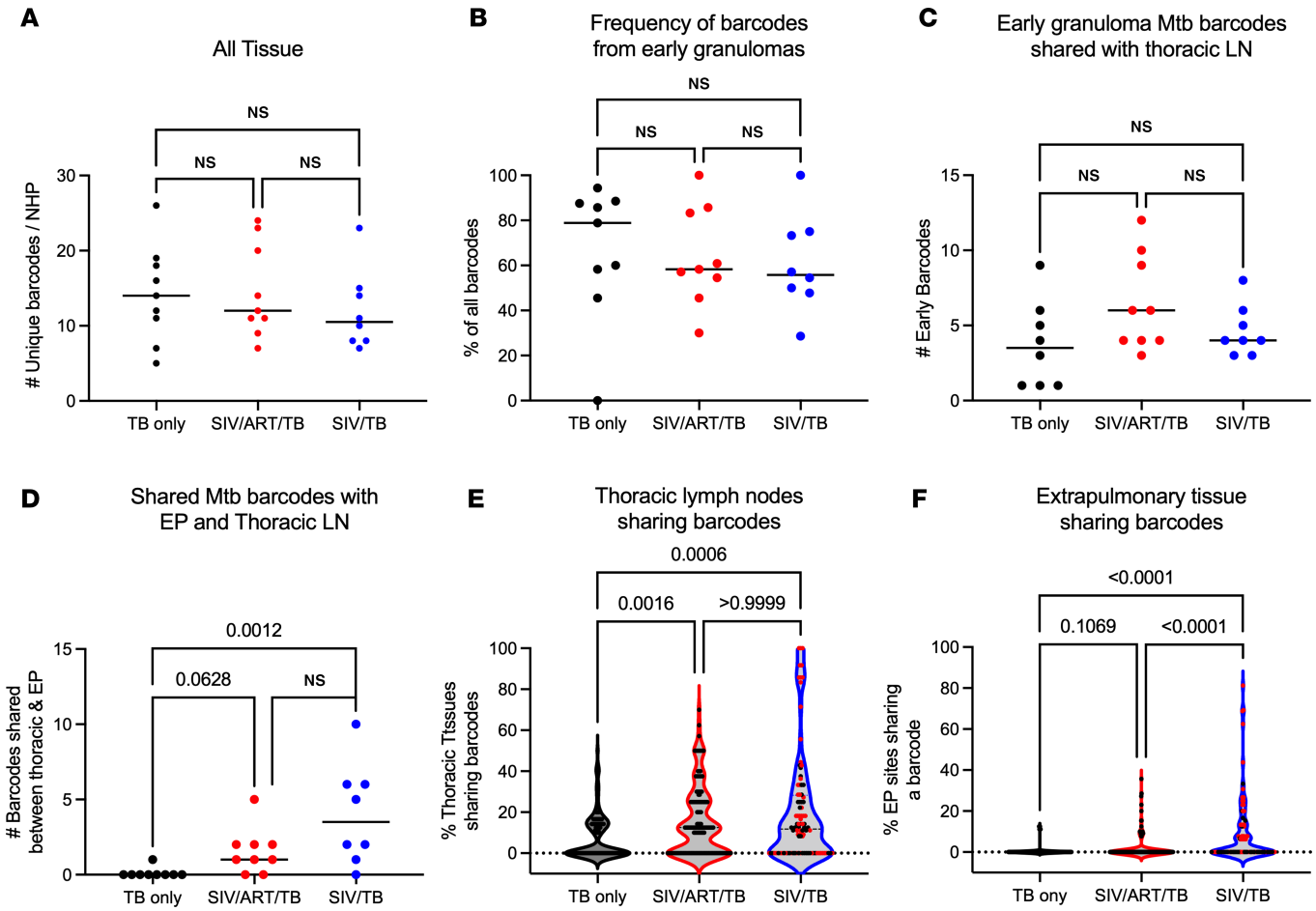

Figure 7. Quantification of barcodes. (**A**) Number unique barcodes in each animal (from all sampled tissues). (**B**) Frequency of barcodes from granulomas seen at 4 weeks after Mtb infection (early). (**C**) Number of barcodes from thoracic lymph nodes that are shared with barcodes from early granulomas. (**D**) Number of barcodes shared between extrapulmonary sites and thoracic lymph nodes. (**A**–**D**) Each dot represents an animal; lines represent medians. TB-only (n = 8–9), SIV/ART/TB (n = 9), SIV/TB (n = 8). (**E**) Proportion of thoracic LN tissues that share barcodes. (**F**) Proportion of extrapulmonary sites that share barcodes. (**E** and **F**) Each dot represents a barcode; red dots indicate barcodes from animals that did not make it to the planned end of study. Kruskal-Wallis test with Dunn's multiple-comparison adjusted P values reported.

ART alone rather than nonreplicative SIV. Unfortunately, we did not have a control group infected with Mtb infection on ART without SIV infection to directly address this. In patients negative for HIV who were treated with tenofovir-based antiretroviral preexposure prophylaxis (PrEP) (58), the frequency and magnitude of blood CD4 and CD8 T cells was similar; however, the expression of CD69 and CCR5 was increased in CD4 and CD8 T cells compared with controls (59). In tissue-specific sites, PrEP also has been shown to induce type I/III IFN pathways in gut tissues that was not observed in PBMC (60) and reduced frequencies of macrophages and $CCR5^{+}CD4^{+}$ T cells in the cervix (59) was also noted in patients negative for HIV. Future investigations are warranted to specifically address this question. Lastly, the rate of the extrapulmonary TB disease in humans is likely severely underestimated, given the lack of diagnostic tools to adequately assess it (50).

Certainly ART has long-term protective effects among PLWHIV (4), and early initiation of ART can reduce the risk of TB (61). The surprising rates of extrapulmonary disease after aggressive ART treatment in our study despite normalized CD4 T cell counts and subtle changes in CD8 T cell function underscore the need to understand the immunologic mechanisms of TB progression and how ART modulates immune responses impaired by HIV. Interestingly, other studies of rhesus macaques with initial asymptomatic Mtb infection and subsequent SIV infection with ART also saw various patterns of increased bacterial burden (though not the same pattern as we saw) despite normalized CD4 T cell counts (28, 29). That said, the sequence of infection (i.e., having HIV infection first or Mtb infection first) likely plays an important role in the mechanisms of bacterial dissemination. Unfortunately, humans

with HIV-TB coinfection are not aware typically of which infection occurred first, which reinforces the importance of these animal models. Further studies are needed to develop better diagnostic and therapeutic strategies in HIV/Mtb coinfected individuals.

Methods

Sex as a biological variable. Our study examined both 28 male and 4 female animals (Supplemental Table 1). More male NHPs were utilized in this study due to availability.

Animals. Adult cynomolgus macaques (*Macaca fascicularis*) (>4 years) (Valley Biosystems) were screened for other comorbidities (e.g., parasites, SIV, Mtb) and then randomly assigned into 4 different experimental groups: TB-only (n = 10), SIV/ART/TB (n = 10), SIV/TB (N = 9), and SIV-only (N = 3) (Figure 1A and Supplemental Table 1). A sample size of 10 animals per treatment group was calculated to detect a difference in lung inflammation of $\log_{10}1.1$ with 80% power ($\alpha = 0.05$). The majority of animals was male due to the limited availability of females. To limit any sex bias, we attempted to ensure that each experimental group had an equal proportion of females across groups. SIV-designated macaques were infected with 7×10^4 IU of SIVB670 (ARP-633, HIV Reagent Program) via i.v. injection. SIVB670 infection was confirmed by detection of plasma SIV RNA. Three days after SIV infection, SIV/ART/TB-designated macaques were treated with tenofovir (20 mg/kg/dose, TFV) and emtricitabine (40 mg/kg/day, FTC) plus dolutegravir (2.5 mg/kg/day, DTG) given via s.c. route daily (30). After 4 months of SIV infection, macaques were infected with a low dose (8–17 CFU per monkey) of digitally barcoded Mtb (Erdman strain) (37) via bronchoscopic instillation to the lower lung lobe and housed in a Biosafety Level 3 (BSL-3) NHP facility, as previously described (21, 22, 27) (Figure 1A). Mtb infection was confirmed by the detection of TB-specific lesions on serial PET-CT scans and confirmed at necropsy. Blood was obtained every 1–4 weeks throughout the course of the study for serial SIV viral load and systemic immune responses, as previously described (21). Bronchoalveolar lavage (BAL) was performed monthly throughout the study.

Peripheral (axillary and inguinal) lymph node biopsies were performed prior to SIV infection, 4 weeks after SIV infection, prior to Mtb infection, and 4 weeks after Mtb infection.

Clinical measurements and scoring. Serial clinical, microbiologic, radiographic, and immunologic metrics were regularly obtained. After Mtb infection, BAL and GA were performed every 4 weeks for Mtb growth and ESR every 2–4 weeks. Daily clinical assessments were conducted and animals that showed evidence of clinical deterioration were monitored and euthanized prior to 12 weeks if they met clinical criteria (i.e., loss of appetite, weight loss, increase in respiratory rate or effort, hunched posture, and dehydration).

Clinical scores were generated by measuring TB specific signs observed from each animal after Mtb infection in 2-week time intervals (0–2 weeks, 2–4 weeks, 4–6 weeks, 6–8 weeks, 8–10 weeks, 10–12 weeks, 12–14 weeks) (31). These signs included: Mtb growth from either GA or BAL, abnormal ESR (>2 mm), coughing, loss of appetite, weight loss, increased respiration, hunched posture, and dehydration. NHP who developed 1, 2, 3, or 4 of these clinical signs of disease during a 2-week time frame were identified.

PET-CT imaging and analysis. To follow in vivo disease progression, serial PET-CT imaging was performed using FDG as the probe to identify TB lesions (62). Animal studies were performed in cohorts over several years with 2 different PET-CT scanners: PET coregistered with CT in the first cohorts were imaged with a microPET Focus 220 preclinical PET (Siemens Medical Solutions) and a CereTom clinical helical CT (NeuroLogica Corp) (22, 26, 63) while the latter cohorts were imaged using a Mediso MultiScan LFER 150 integrated preclinical PET-CT (Mediso).

Each PET scanner's sensitivity was calibrated by the respective manufacturer's recommended procedure, involving scan measurements of known quantities of radioactivity within known volumes of solution. All quantities of tracer, for both the purpose of calibration and scientific measurement, were measured with the same dose calibrator. PET-CT scans were performed every 4 weeks after Mtb infection. As previously described (64), Mtb involvement within the lungs and thoracic lymph nodes was measured using several different parameters, such as count of individual granulomas, total lung FDG activity, number of mediastinal lymph nodes with increased FDG avidity with or without the presence of necrosis, and presence of extrapulmonary involvement (e.g., liver lesions), as previously described (22, 65).

Plasma sCD14 and sCD163 measurements. Levels of sCD14 (R&D Systems, Human sCD14 ELISA, Bio-Techne) and sCD163 (MyBiosource, Monkey sCD163 ELISA) were measured by commercial kits. Plasma samples from animals were obtained at serial time points and filtered (0.22 μm) prior to freezing

(–80°C). Samples were then thawed, diluted (1:100 for sCD163, 1:400 for sCD14) in diluting buffer and run according to manufacturer's instruction. Samples were run in duplicate. Optimal densities were measured using Spectramax Microplate Reader 190 (Molecular Devices) using analysis software (SoftMax-Pro 7.1.2). Analysis of the sCD14 and sCD163 standards were transformed using 4 parameter logistic regression and linear regression methods, respectively.

Necropsy. TB-specific gross pathology at the time of necropsy was quantified using a gross pathology score system that accounts for the number and size of granulomas, distribution of disease (e.g., lung lobes, lymph nodes, extrapulmonary sites) previously described (66). PET-CT matched lesions were harvested and halved for histopathology and homogenized into single-cell suspensions for bacterial burden and killing and immunology as previously described (22, 64).

Ex vivo immunologic assays. Flow cytometry was used to determine phenotypic and functional changes in CD4 and CD8 T cells from PBMC, BAL, and peripheral lymph nodes over time. Cells were stimulated with ESAT6 and CFP10 peptides or SIV Gag-Pol peptide pools Mtb (10 μg/mL) in media (RPMI+10% hAB), media alone, or PBDU/ionomycin (BEI Resources). PBMC were stimulated for 6 hours, while BAL samples were stimulated for 4 hours in the presence of Brefeldin A. Tissue samples were incubated with media alone and Brefeldin A for 4 hours. Flow cytometry was performed on all stimulated cells after staining with a combination of antibodies (Supplemental Table 2). Data acquisition was performed using an LSR II (BD) and analyzed using FlowJo Software v.10.8 (Treestar Inc.) using a standardize gating strategy (Supplemental Figure 12).

SIV RNA isolation and quantification from plasma and tissues. Viral RNA was isolated from plasma as previously described (55). Briefly, plasma was separated from EDTA-treated whole blood and stored at –80°C until use. Plasma was centrifuged at 16,000*g* for 1 hour at 4°C. The viral pellet was resuspended in 5 mM Tris-HCl (pH 8.0) containing 200 μg of proteinase K for 30 minutes at 55°C, followed by 5.8M guanidinium isothiocyanate containing 200 μg of glycogen. RNA was precipitated with isopropanol, washed with 70% ethanol and resuspended in 5 mM Tris-HCl (pH 8.0) containing 1 μM dithiothreitol and 1,000 U of an RNase inhibitor (RNasin; ThermoFisher) and stored at –80°C until use.

Tissue-specific RNA was isolated from single-cell homogenates stored in Trizol LS. After thawing, the homogenate was mixed with 1-bromo-3-chloropropane (MRC Labs) at 10:1 and centrifuged at 14,000*g* for 15 minutes at 4°C. The upper aqueous phase was removed to a new tube and 240 mg glycogen (Roche) was added. Isopropanol was added and mixed before centrifugation at 21,000*g* for 10 minutes at room temperature. The pellet was washed with 70% ethanol and centrifuged at 21,000*g* for 5 minutes at room temperature. After the final wash, the pellet was dried, resuspended in RNase-free water, and stored at –80°C until use.

qPCR was performed as previously reported (67). Briefly, cDNA synthesis was performed on the isolated RNA using SuperScript III First-Strand Synthesis SuperMix (ThermoFisher) following manufacturer's instructions and using supplied random hexamers. qPCR was performed in duplicate wells using SsoAdvanced Universal Probes Supermix (Bio-Rad). Primers and probes were designed for macaque CD4 (tissues only), as previously described (67) and SIVB670 *gag*: forward 5′-GTCTGCGTCATTTGGTGCATTC-3′, reverse 5′-CACTAGATGTCTCTGCACTATTTGTTTTG-3′, and Probe FAM-CGCAGAAGAGAAAGTGAAACATACTGAGGAAG-TAMRA. Viremia is reported as SIV RNA copies per mL (plasma) or copies per 1×10^6 CD4 RNA copies (tissues).

Quantification of Mtb viable and total (genomic) bacterial burden. Colony forming units (CFU) were used to estimate bacterial growth within single-cell homogenates from each individual site, as previously described (22, 23, 66). The sum of CFU within lymph nodes was considered lymph node burden ("LN CFU") and was defined as the sum of CFU from all thoracic lymph nodes. We quantified extrapulmonary involvement (EP score) through TB disease in EP sites (e.g., liver, peripancreatic lymph node, paracostal abscess, kidney) for which bacterial growth, gross, or microscopic evidence of Mtb involvement were observed (22, 66). Total bacterial burden includes the sum of CFU from the lymph nodes (mediastinal and extrapulmonary) and lung lesions (e.g., grossly normal lung, granulomas, involved lung, or diaphragm granulomas), as previously described (22, 66).

Mtb DNA extractions and qPCR for estimating chromosomal equivalents (CEQ) (estimated live and dead Mtb) were performed as previously described (22, 35). CEQ were assessed relative to a serially diluted standard curve of Mtb genomic DNA using qPCR; efficiency for each run was kept between 90% and 110%. Each sample was analyzed in duplicate on a QuantStudio 6 real-time PCR system (ThermoFisher Scientific) with a 96-well block using primers targeting SigF and iTaq Universal SYBR Green Supermix (Bio-Rad).

t-SNE analysis. Flow cytometry data of gated lymphocytes from SIV/TB (n = 3), SIV/ART/TB (n = 3), and TB-only (N = 2) NHPs were concatenated into single FCS files in FlowJo 10 software based on individual cohort for lung granulomas and thoracic LN. The numbers of granulomas included within the concatenation file were 39, 43, and 19 in SIV/TB, SIV/ART/TB, and TB-only NHPs, respectively. The numbers of thoracic lymph nodes included in the concatenated file were 12, 14, and 4 in SIV/TB, SIV/ART/TB, and TB-only NHPs, respectively. The concatenated files were downsampled to 250,000 events per cohort, and t-SNE–CUDA visualization was performed in Cytobank. Perplexity and the number of iterations were automatically applied. The antibodies utilized for t-SNE analysis were CD3, CD4, CD8, CD38, HLA-DR, TNF, IFN-γ, IL-2, CD107a, IL-17, and IL-10.

Plasma cytokine and chemokine detection. Plasma cytokine and chemokine measurements from animals were performed using the Meso Scale Discovery (MSD) per V-PLEX NHP Cytokine 24-Plex kit (K15058D-2) packaged instruction. The following were examined: IL-12/IL-23p40, IL-2, IP-10, MCP-4, IL-15, MCP-1, IL-6, MIP-1α, IL-7, IL-8, MIP-1a, GM-CSF, TNF-α, IL-8 (HA), Eotaxin-3, IL-16, IL-5, MDC, IFN-γ, and VEGF. All samples were plated as neat. Results are displayed with https://software.broadinstitute.org/morpheus/.

Barcode diversity. Diversity of mycobacterial DNA barcodes was quantified using the effective number of species, calculated from the Shannon entropy index (57). The effective number was broken down by anatomical compartment and barcode diversity within lung lobes are reported.

Barcode determination to track Mtb dissemination and Circos plots. To track Mtb dissemination, digitally barcoded Mtb was used as previously described (37). Each library contained approximately 16,000 unique barcodes and 3 independently generated libraries were combined into a master library to increase the number of unique barcodes, ensuring a < 2% chance that a barcode would be represented twice if 20 bacteria are randomly selected (37). Scan matched lesions and other tissues were plated for viable Mtb growth after which purified bacterial DNA was extracted using phenol-chloroform methods. DNA barcodes in each sample were amplified using PCR and quantified, as described in ref. 68. Briefly, purified bacterial genomic DNA was diluted to 10 ng/μL in dH_2O and amplified with Q5 polymerase (catalog M0491; New England Biolabs) in 2 rounds of PCR to amplify barcode sequences and introduce Illumina adaptor sequences. Then, amplified dual-indexed product was purified using AMPure XP beads (catalog A63881; Beckman Coulter) and samples pooled to a final concentration of 8 pM (concentration checked using Kapa Library Quantification Kit (catalog KK4824; Roche) before spiking with 20% PhiX control library (Illumina) to increase sequencing diversity. The pool was sequenced on the Illumina MiSeq system using V2 chemistry for 300 cycles. Typical total reads from a library are around 40 million with 35 million PF reads (passed illumina filter), and each individual tissue sample should make up 1%–3% of the total PF reads.

After sequencing, samples were demultiplexed on Basespace (Illumina), and resulting Fastq files were analyzed using custom Perl scripts to quantify individual barcodes in each sample (58). Briefly, the script required that a sample had more than 10,000 total reads and searched Read 1 sequences for 3 motifs indicative of a valid barcoded strain. To eliminate reads with putative sequencing errors and chimera sequences (in which a read contains a qTag that is associated with a different barcode than it should), reads with lower counts that differed by 1 base pair from another higher counted barcode were deleted. This was iteratively done for all barcodes in the list. The remaining barcodes and counts in the list were $\log_2$ transformed, and the second derivate of rank-ordered data was calculated for each pair of normalized adjacent counts in the list (e.g., counts 1,2; 2,3; and 3,4). The lowest value is used to separate true counts from the background. Finally, every sample's analysis was manually reviewed to ensure consistency and check for aberrant sequences such as missed chimeras. The resulting data consist of tables that quantify all unique barcodes in a batch of samples on the same sequencing run and the fraction of reads assigned to each barcode in a sample. All scripts and instructions for executing these analyses are publicly available on Github (https://github.com/sarahfortunelab/barcodetracking; commit ID f1e07b5a1dfe27d270b4cdb7c70b107b5ba2bdb3).

Generating Circos plots from barcoding data. Using the resulting tables of identified barcodes for each NHP, we further translated this data into a configuration file of dissemination compatible with plotting with the Circos software (69). Specifically, using 4 custom Python scripts, we successively performed the following data transformations by (a) identifying and coloring bands representing different barcodes present in each tissue; (b) generating outside highlight tracks that are colored by anatomical site; (c) creating a table of tissues that are linked by ribbons representing dissemination across tissues; and (d) deriving a text insert describing the coordinates and colors of the ribbons to be pasted into the Circos configuration

file. Additionally, we manually created tab-delimited Circos-compatible text files that highlighted the time of PET-CT lesion detection and the log-transformed CFUs in each tissue at necropsy. Finally, each plot was manually adjusted such that links between tissues sharing barcodes were drawn, when possible, to originate from lung sites detected early by PET-CT with the highest CFU burden; however, other lung sites with the same barcode may also be the source of dissemination between tissues. If no tissue in a barcode dissemination network was identified at 4 weeks after infection, the tissue with the highest CFU burden was chosen as the origin site. All barcode matrices for each NHP and custom scripts for Circos plot generation are publicly available on Github (https://github.com/Fortune-Lab/nhp_circos_plots; commit ID e147447c59a590c2962614a33c474ada286857b9).

Statistics. Data were tested for normality with Shapiro-Wilk test. Multiple Mann-Whitney *U* tests with Holm-Šídák adjusted *P* values were used to analyze 2 groups over time. Wilcoxon matched-pairs signed-rank test was used to test differences among paired data points. When testing mean differences among 3 groups, 1-way ANOVA with Tukey's multiple-comparison adjustment was used for normally distributed data; otherwise, Kruskal-Wallis test with Dunn's multiple-comparison adjustment was used. Lung inflammation over time was compared across groups using 2-way ANOVA with Tukey's multiple-comparison adjustment (for comparing all 3 groups at each time point). For categorical data, Fisher's exact test was used to compare distributions among treatment groups. Statistical tests above were performed in GraphPad Prism Mac OSX (Version 10.3.1, GraphPad). For multiple granulomas and thoracic lymph nodes per animal, random effect models (monkey as the random effect and treatment group as the fixed effect) were fit using the restricted maximum likelihood (REML) method (JMP Pro 17.2.0). Tukey honestly significant difference (HSD) adjusted *P* values are reported for pair-wise multiple comparisons. All statistical tests are 2 sided, and significance was established at $P < 0.05$ and trends $P < 0.10$.

Study approval. All animal procedures were approved by the University of Pittsburgh IACUC in compliance with the Animal Welfare Act and Guide for the Care and Use of the Laboratory Animals.

Data availability. All data points are reported in the Supporting Data Values file. Custom Python scripts for barcode tracking and Circos plots are provided in https://github.com/sarahfortunelab/barcodetracking (commit ID f1e07b5a1dfe27d270b4cdb7c70b107b5ba2bdb3), and https://github.com/Fortune-Lab/nhp_circos_plots (commit ID e147447c59a590c2962614a33c474ada286857b9).

Author contribution

ZA and PLL conceived project, developed protocols, designed, analyzed, and interpreted experiments and wrote the manuscript. CRD performed, analyzed, and interpreted experiments, and wrote the manuscript. TR, JL Gleim, JMM, JL Gaines, FH, CK, EK, DF, KK, JT, JS, and JEK performed and analyzed experiments. HJB, HBC, and PM performed data, imaging, diversity, and statistical analyses. SMF, MCC, JLF performed, analyzed, and interpreted experiments. All authors reviewed and edited the manuscript.

Funding support

This work is the result of NIH funding, in whole or in part, and is subject to NIH Public Access Policy. Through acceptance of this federal funding, the NIH has been given the right to make the work publicly available in PubMed Central.

- NIH NIAID-R01 AI11871 and R01 AI134195 to PLL.
- NIH NIAID-UC7AI180311.
- NIH NIAID-R01-AI155495 to PLL.

Acknowledgments

We thank the laboratory and veterinary technicians of the Lin, Flynn, and Scanga Research Laboratories for their intellectual contributions and dedicated work.

Address correspondence to: Philana Ling Lin, UPMC Children's Hospital of Pittsburgh 2310 AOB, 4401 Penn Ave., Pittsburgh, Pennsylvania, 15224, USA. Phone: 412.383.2178; Email: linpl@chp.edu.

1. World Health Organization. Global Tuberculosis Report 2025. https://www.who.int/teams/global-programme-on-tuberculosis-and-lung-health/tb-reports/global-tuberculosis-report-2025. Accessed January 28, 2026.
2. Bell LCK, Noursadeghi M. Pathogenesis of HIV-1 and Mycobacterium tuberculosis co-infection. *Nat Rev Microbiol*. 2018;16(2):80–90.

3. Jones BE, et al. Relationship of the manifestations of tuberculosis to CD4 cell counts in patients with human immunodeficiency virus infection. *Am Rev Respir Dis*. 1993;148(5):1292–1297.
4. Mohammed H, et al. Prevalence of extrapulmonary tuberculosis among people living with HIV/AIDS in sub-Saharan Africa: a systeic review and meta-analysis. *HIV AIDS (auckl)*. 2018;10:225–237.
5. Sterling TR, et al. HIV infection-related tuberculosis: clinical manifestations and treatment. *Clin Infect Dis*. 2010;50 Suppl 3:S223–S230.
6. Tornheim JA, Dooley KE. Tuberculosis associated with HIV infection. *Microbiol Spectr*. 2017;5(1).
7. Lawn SD, Wilkinson RJ. ART and prevention of HIV-associated tuberculosis. *Lancet HIV*. 2015;2(6):e221–e222.
8. Suwanpimolkul G, et al. Incidence of active tuberculosis among people living with HIV receiving long-term antiretroviral therapy in high TB/HIV burden settings in Thailand: implication for tuberculosis preventive therapy. *J Int AIDS Soc*. 2022;25(4):e25900.
9. Johansen IS, et al. Risk of tuberculosis after initiation of antiretroviral therapy among persons with HIV in Europe. *Int J Infect Dis*. 2024;147:107199.
10. Liu E, et al. Tuberculosis incidence rate and risk factors among HIV-infected adults with access to antiretroviral therapy. *AIDS*. 2015;29(11):1391–1399.
11. Takarinda KC, et al. Declining tuberculosis case notification rates with the scale-up of antiretroviral therapy in Zimbabwe. *Public Health Action*. 2016;6(3):164–168.
12. Lawn SD, Churchyard G. Epidemiology of HIV-associated tuberculosis. *Curr Opin HIV AIDS*. 2009;4(4):325–333.
13. Suthar AB, et al. Antiretroviral therapy for prevention of tuberculosis in adults with HIV: a systematic review and meta-analysis. *PLoS Med*. 2012;9(7):e1001270.
14. Chiacchio T, et al. Impact of antiretroviral and tuberculosis therapies on $CD4^+$ and $CD8^+$ HIV/M. tuberculosis-specific T-cell in co-infected subjects. *Immunol Lett*. 2018;198:33–43.
15. Correa-Macedo W, et al. Alveolar macrophages from persons living with HIV show impaired epigenetic response to Mycobacterium tuberculosis. *J Clin Invest*. 2021;131(22):e148013.
16. Girardi E, et al. Impact of previous ART and of ART initiation on outcome of HIV-associated tuberculosis. *Clin Dev Immunol*. 2012;2012:931325.
17. Lawn SD, et al. Antiretroviral therapy and the control of HIV-associated tuberculosis. Will ART do it? *Int J Tuberc Lung Dis*. 2011;15(5):571–581.
18. Uthman OA, et al. Optimal timing of antiretroviral therapy initiation for HIV-infected adults with newly diagnosed pulmonary tuberculosis: a systematic review and meta-analysis. *Ann Intern Med*. 2015;163(1):32–39.
19. Webb Mazinyo E, et al. Adherence to concurrent tuberculosis treatment and antiretroviral treatment among co-infected persons in South Africa, 2008-2010. *PLoS One*. 2016;11(7):e0159317.
20. Bucsan AN, et al. Mechanisms of reactivation of latent tuberculosis infection due to SIV coinfection. *J Clin Invest*. 2019;129(12):5254–5260.
21. Diedrich CR, et al. Reactivation of latent tuberculosis in cynomolgus macaques infected with SIV is associated with early peripheral T cell depletion and not virus load. *PLoS One*. 2010;5(3):e9611.
22. Diedrich CR, et al. SIV and Mycobacterium tuberculosis synergy within the granuloma accelerates the reactivation pattern of latent tuberculosis. *PLoS Pathog*. 2020;16(7):e1008413.
23. Foreman TW, et al. $CD4^+$ T-cell-independent mechanisms suppress reactivation of latent tuberculosis in a macaque model of HIV coinfection. *Proc Natl Acad Sci U S A*. 2016;113(38):E5636–E5644.
24. Foreman TW, et al. CD4 T cells are rapidly depleted from tuberculosis granulomas following acute SIV co-infection. *Cell Rep*. 2022;39(9):110896.
25. Capuano SV, et al. Experimental Mycobacterium tuberculosis infection of cynomolgus macaques closely resembles the various manifestations of human M. tuberculosis infection. *Infect Immun*. 2003;71(10):5831–5844.
26. Lin PL, et al. Quantitative comparison of active and latent tuberculosis in the cynomolgus macaque model. *Infect Immun*. 2009;77(10):4631–4642.
27. Corleis B, et al. HIV-1 and SIV infection are associated with early loss of lung interstitial $CD4^+$ T cells and dissemination of pulmonary tuberculosis. *Cell Rep*. 2019;26(6):1409–1418.
28. Sharan R, et al. Antiretroviral therapy timing impacts latent tuberculosis infection reactivation in a Mycobacterium tuberculosis/SIV coinfection model. *J Clin Invest*. 2022;132(3):e153090.
29. Ganatra SR, et al. Antiretroviral therapy does not reduce tuberculosis reactivation in a tuberculosis-HIV coinfection model. *J Clin Invest*. 2020;130(10):5171–5179.
30. Whitney JB, et al. Rapid seeding of the viral reservoir prior to SIV viraemia in rhesus monkeys. *Nature*. 2014;512(7512):74–77.
31. Medrano JM, et al. Characterizing the spectrum of latent Mtb infection in the cynomolgus macaque model: Clinical, immunologic, and PET-CT features of evolution. *J Infect Dis*. 2023;227(4):592–601.
32. Meng Q, et al. Immune activation at sites of HIV/TB co-infection contributes to the pathogenesis of HIV-1 disease. *PLoS One*. 2016;11(11):e0166954.
33. Gideon HP, et al. Variability in tuberculosis granuloma T cell responses exists, but a balance of pro- and anti-inflammatory cytokines is associated with sterilization. *PLoS Pathog*. 2015;11(1):e1004603.
34. Hiza H, et al. CD38 expression by antigen-specific CD4 T cells is significantly restored 5 months after treatment initiation independently of sputum bacterial load at the time of tuberculosis diagnosis. *Front Med (Lausanne)*. 2022;9:821776.
35. Ganchua SKC, et al. Lymph nodes are sites of prolonged bacterial persistence during Mycobacterium tuberculosis infection in macaques. *PLoS Pathog*. 2018;14(11):e1007337.
36. Moriarty RV, et al. Spontaneous control of SIV replication does not prevent T cell dysregulation and bacterial dissemination in animals co-infected with M. tuberculosis. *Microbiol Spectr*. 2022;10(3):e0172421.
37. Martin CJ, et al. Digitally barcoding *Mycobacterium tuberculosis* reveals *In Vivo* infection dynamics in the macaque model of tuberculosis. *mBio*. 2017;8(3):e00312-17.
38. Williams PM, et al. Tuberculosis - United States, 2023. *MMWR Morb Mortal Wkly Rep*. 2024;73(12):265–270.
39. Behr MA, et al. Revisiting the timetable of tuberculosis. *BMJ*. 2018;362:k2738.

40. van der Spuy GD, et al. Use of genetic distance as a measure of ongoing transmission of Mycobacterium tuberculosis. *J Clin Microbiol*. 2003;41(12):5640–5644.
41. Verver S, et al. Transmission of tuberculosis in a high incidence urban community in South Africa. *Int J Epidemiol*. 2004;33(2):351–357.
42. Guo M, et al. SIV infection facilitates *Mycobacterium tuberculosis* infection of rhesus macaques. *Front Microbiol*. 2016;7:2174.
43. Larson EC, et al. Host immunity to Mycobacterium tuberculosis infection is similar in simian immunodeficiency virus (SIV)-infected, antiretroviral therapy-treated and SIV-naïve juvenile macaques. *Infect Immun*. 2023;91(5):e0055822.
44. Rodgers MA, et al. Preexisting simian immunodeficiency virus infection increases susceptibility to tuberculosis in Mauritian Cynomolgus macaques. *Infect Immun*. 2018;86(12):e00565-18.
45. Lawson L, et al. Clinical presentation of adults with pulmonary tuberculosis with and without HIV infection in Nigeria. *Scand J Infect Dis*. 2008;40(1):30–35.
46. Wood R, et al. Risk factors for developing tuberculosis in HIV-1-infected adults from communities with a low or very high incidence of tuberculosis. *J Acquir Immune Defic Syndr*. 2000;23(1):75–80.
47. Tippalagama R, et al. HLA-DR marks recently divided antigen-specific effector CD4 T cells in active tuberculosis patients. *J Immunol*. 2021;207(2):523–533.
48. Kgoadi K, et al. Alveolar macrophages from persons with HIV mount impaired TNF signaling networks to M. tuberculosis infection. *Nat Commun*. 2025;16(1):2397.
49. Behr MA, Waters WR. Is tuberculosis a lymphatic disease with a pulmonary portal? *Lancet Infect Dis*. 2014;14(3):250–255.
50. Rodriguez-Takeuchi SY, et al. Extrapulmonary tuberculosis: pathophysiology and imaging findings. *Radiographics*. 2019;39(7):2023–2037.
51. Shivakoti R, et al. Association of HIV infection with extrapulmonary tuberculosis: a systematic review. *Infection*. 2017;45(1):11–21.
52. Seraphin MN, et al. Association between Mycobacterium tuberculosis lineage and site of disease in Florida, 2009-2015. *Infect Genet Evol*. 2017;55:366–371.
53. Naing C, et al. Meta-analysis: the association between HIV infection and extrapulmonary tuberculosis. *Lung*. 2013;191(1):27–34.
54. Arpagaus A, et al. Extrapulmonary tuberculosis in HIV-infected patients in rural Tanzania: the prospective Kilombero and Ulanga antiretroviral cohort. *PLoS One*. 2020;15(3):e0229875.
55. Hoogendoorn JC, et al. Reduction in extrapulmonary tuberculosis in context of antiretroviral therapy scale-up in rural South Africa. *Epidemiol Infect*. 2017;145(12):2500–2509.
56. Mankatittham W, et al. Characteristics of HIV-infected tuberculosis patients in Thailand. *Southeast Asian J Trop Med Public Health*. 2009;40(1):93–103.
57. Benlarbi M, et al. Plasma human immunodeficiency virus 1 soluble glycoprotein 120 association with correlates of immune dysfunction and inflammation in antiretroviral therapy-treated individuals with undetectable viremia. *J Infect Dis*. 2024;229(3):763–774.
58. Pattacini L, et al. Antiretroviral pre-exposure prophylaxis does not enhance immune responses to HIV in exposed but uninfected persons. *J Infect Dis*. 2015;211(12):1943–1952.
59. Richert-Spuhler LE, et al. Pre-exposure prophylaxis differentially alters circulating and mucosal immune cell activation in herpes simplex virus type 2 seropositive women. *AIDS*. 2019;33(14):2125–2136.
60. Hughes SM, et al. Treatment with commonly used antiretroviral drugs induces a type I/III interferon signature in the gut in the absence of HIV infection. *Cell Rep Med*. 2020;1(6):100096.
61. Blanc F-X, et al. Earlier versus later start of antiretroviral therapy in HIV-infected adults with tuberculosis. *N Engl J Med*. 2011;365(16):1471–1481.
62. Lin PL, et al. Radiologic responses in cynomolgus macaques for assessing tuberculosis chemotherapy regimens. *Antimicrob Agents Chemother*. 2013;57(9):4237–4244.
63. Sarnyai Z, et al. Performance evaluation of a high-resolution nonhuman primate PET/CT system. *J Nucl Med*. 2019;60(12):1818–1824.
64. White AG, et al. Analysis of 18FDG PET/CT imaging as a tool for studying Mycobacterium tuberculosis infection and treatment in non-human primates. *J Vis Exp*. 2017;127:56375.
65. Lin PL, et al. PET-CT identifies reactivation risk in cynomolgus macaques with latent M. tuberculosis. *PLoS Pathog*. 2016;12(7):e1005739.
66. Maiello P, et al. Rhesus macaques are more susceptible to progressive tuberculosis than cynomolgus macaques: a quantitative comparison. *Infect Immun*. 2018;86(2):e00505-17.
67. Kline C, et al. Persistence of viral reservoirs in multiple tissues after antiretroviral therapy suppression in a macaque RT-SHIV model. *PLoS One*. 2013;8(12):e84275.
68. Winchell CG, et al. $CD8^+$ lymphocytes are critical for early control of tuberculosis in macaques. *J Exp Med*. 2023;220(12):e20230707.
69. Krzywinski M, et al. Circos: an information aesthetic for comparative genomics. *Genome Res*. 2009;19(9):1639–1645.